

# Diff-Def: Diffusion-Generated Deformation Fields for Conditional Atlases

Sophie Starck<sup>\*1</sup>, Vasiliki Sideri-Lampretsa<sup>\*1</sup>, Bernhard Kainz<sup>3,4</sup>, Martin Menten<sup>1,3</sup>, Tamara Mueller<sup>\*1,2</sup>, and Daniel Rueckert<sup>\*1,3</sup>

<sup>1</sup> School of Computation, Information and Technology and School of Medicine, Klinikum rechts der Isar, Technical University of Munich

<sup>2</sup> Department of Diagnostic and Interventional Radiology, School of Medicine, Klinikum rechts der Isar, Technical University of Munich

<sup>3</sup> Department of Computing, Imperial College London

<sup>4</sup> FAU Erlangen-Nürnberg, Germany

[sophie.starck@tum.de](mailto:sophie.starck@tum.de), [vasiliki.sideri-lampretsa@tum.de](mailto:vasiliki.sideri-lampretsa@tum.de)

**Abstract.** Anatomical atlases are widely used for population analysis. Conditional atlases target a particular sub-population defined via certain conditions (e.g. demographics or pathologies) and allow for the investigation of fine-grained anatomical differences – such as morphological changes correlated with age. Existing approaches use either registration-based methods that are unable to handle large anatomical variations or generative models, which can suffer from training instabilities and hallucinations. To overcome these limitations, we use latent diffusion models to generate *deformation fields*, which transform a general population atlas into one representing a specific sub-population. By generating a deformation field and registering the conditional atlas to a neighbourhood of images, we ensure structural plausibility and avoid hallucinations, which can occur during direct image synthesis. We compare our method to several state-of-the-art atlas generation methods in experiments using 5000 brain as well as whole-body MR images from UK Biobank. Our method generates highly realistic atlases with smooth transformations and high anatomical fidelity, outperforming the baselines.

## 1 Introduction

Anatomical atlases –also called templates– represent an average anatomy of a population in the form of intensity templates or probabilistic maps. They provide a common coordinate system for all images of a cohort and allow for an investigation of inter-subject variability and population differences, as well as anomaly detection [2,11,16,8,4,5]. An atlas that best represents a whole population should ideally have a minimal distance to every subject in the dataset. However, a single general atlas for the whole cohort might not be able to capture the variability between sub-groups, e.g. morphological differences that occur with age. As a

---

<sup>\*</sup> These authors contributed equally to this work

result, conditional atlases have been introduced to represent a sub-population with specific characteristics (e.g. demographics such as age or sex).

Current approaches to create conditional atlases are either based on (a) iteratively registering images of a sub-group to a reference image or by (b) employing generative models that directly learn the atlas [10,12,20]. Usually, the former employs deformable registration [30], where semantic regions of an image of a cohort and a reference image are aligned and averaged [30]. These methods output a *deformation field*, which maps the image to the atlas and can be further used to quantify anatomical variability and interpret the structural changes. However, this conventional approach is time-consuming since, for each condition, pairwise registration needs to be recomputed [16,31,8]. Conversely, generative models paired with registration show promising results while being faster during inference. However, some of them are greatly affected by training instabilities, hallucinations, and the registration quality, e.g. due to the choice of an inadequate transformation model, potentially leading to low-quality atlases.

In this work, we propose to combine the best of both worlds. We formulate the task of conditional atlas construction as a *deformation field* generation process using Diffusion Denoising Probabilistic Models (DDPM) [15]. The generated deformation field is used to transform a general population atlas into one representing the sub-group, which is characterised by some desired attributes, e.g. age or body mass index (BMI). To ensure a smooth, anatomically faithful appearance, we constrain the conditional atlas to represent best the neighbourhood of images satisfying the attribute of interest. Additionally, by generating a deformation field, the whole method is intrinsically interpretable. Our core contributions can be summarised as follows:

1. We utilise diffusion models to generate an interpretable deformation field which transforms a general population atlas into a conditional atlas.
2. We ensure the construction of a plausible atlas by minimising the distance between the conditional atlas and a neighbourhood of images.
3. We demonstrate the utility of our method by generating brain atlases conditioned on age and CSF volume as well as whole-body atlases of different body compositions.

## 2 Related Work

**Atlas construction** Atlas creation has been performed by iteratively registering all cohort images to a reference image and averaging them [13]. However, this process is time-consuming and leads to low-quality, blurry atlases that do not capture the details of the underlying structural variability [5]. Furthermore, the selection of a reference image introduces a morphological bias to the appearance of the atlas [22,33], requiring an additional unbiasing post-processing step [16] –further increasing the overall processing time. When generating conditional atlases with these methods, only a subset of the data is used for each atlas [31]. This potentially inhibits the ability to learn features across subsets, and its effectiveness is highly dependent on the decision of the demographic attributes.

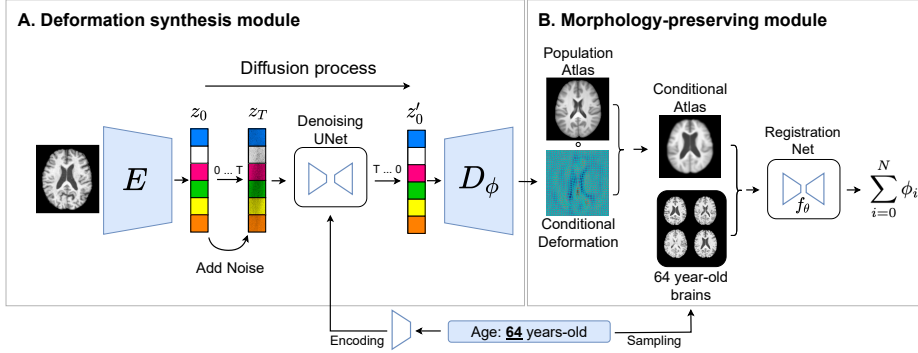


Fig. 1: **Overview of the proposed method.** The Deformation-synthesis module (**A**) generates a deformation field that maps a general population atlas to a conditional atlas. The morphology-preserving module (**B**) ensures structural correctness by minimising the distance to images that satisfy the condition.

More recently, generative methods have also become popular in the context of atlas generation. They eliminate the additional unbiasing step by learning a conditional atlas without explicitly averaging aligned images [10,12,20]. They are trained with either classic registration objectives [10] or generative adversarial networks (GANs) [12]. Dalca et al. [10] propose a network that generates a conditional diffeomorphic (differentiable, invertible, and smooth) atlas. However, the diffeomorphic transformation model may be inadequate, resulting in lower quality atlases due to the intricate nature of human anatomy, which is often non-smooth, e.g. when registering healthy to pathological images. To address this, Dey et al. [12] propose a GAN-based model, combined with non-diffeomorphic registration, that simultaneously minimises a registration and an adversarial loss. However, GANs are challenging to deploy as they suffer from training instabilities and mode collapse [3,14,21]. For these reasons, we leverage the capabilities of diffusion models in this work.

**Diffusion models** Score-based diffusion models, and more specifically, denoising diffusion probabilistic models (DDPMs) [15], have shown remarkable performance in generative modelling in various computer vision fields [9]. While they are capable of yielding high-fidelity data, they also provide attractive properties such as scalability and training tractability. Diffusion models have been used in the medical imaging domain for tasks such as conditional synthetic brain generation [24], anomaly detection [7], and registration [18,25]. These methods are able to generate an unprecedented level of realistic images but still suffer from potential hallucinations. We propose to address this by generating deformation fields instead of images. While [18,25] propose this in the context of pairwise image registration, we introduce deformation field synthesis for conditional atlas generation.

### 3 Methods

**Conditional Latent Diffusion Models (LDMs)** Our proposed method (Figure 1) leverages the flexible and powerful conditional LDM [27] to generate high-resolution 3D *deformation vector fields* (DVF) that transform a general population atlas to fit the conditioning characteristics. We first pre-train an autoencoder (AE) to learn a compressed latent representation  $z$  for each image, where  $E_a$ ,  $D_a$  describe the encoder and decoder of the AE, respectively. Next, we utilise a Denoising Diffusion Probabilistic Model (DDPM) [15]. Here, in the forward process, Gaussian noise  $\mathcal{N}(0, 1)$  is iteratively introduced to the latent variable through a fixed Markov chain. During the reverse process, also modelled as a Markov chain, the model processes Gaussian noise as well as a conditional vector based on the attributes of the sub-population of interest.

**Deformation synthesis module** The desired conditional deformation field is then synthesised by feeding the denoised latent vector  $z'_0$  to a deformation decoder  $D_\phi$ . Instead of following the typical approach of image generation with LDMs, which involves utilising the pre-trained and fixed decoder  $D_a$ , we propose to fine-tune the  $D_a$  to output a DVF ( $D_\phi$ ). This way, we retain meaningful cues learned during the image decompression while learning the desired projection to the deformation domain.

**Morphology-preserving module** The conditional deformation fields generated by the diffusion process allow us to flexibly deform a general population atlas to align with the images that satisfy the feature of interest. To ensure the generation of a smooth, geometrically plausible deformation field, we introduce a morphology-preserving module based on deformable registration. Every epoch, we randomly sample a neighbourhood of  $N$  images that satisfies the condition  $c$  and utilise a pre-trained registration method, Voxelmorph [6], to register each of the neighbourhood’s images to the conditional atlas. This geometry-preserving loss 1 is then calculated by minimising the average deformation of each neighbouring image to the conditional atlas. Thus, this module pushes the generated conditional atlas towards being the most representative point of the attribute-specific neighbourhood and that its distance to each image is minimised. This is described by the following morphology-preserving objective term:

$$\mathcal{L}_{geom} = \frac{1}{N} \sum_{i=1}^N f_\theta(\mathcal{A}_{MNI} \circ \phi_c, \mathcal{N}_i). \quad (1)$$

Here,  $\mathcal{A}_{MNI}$  is the general population atlas deformed by the diffusion-generated conditional deformation field  $\phi_c$ ,  $\mathcal{N}_i$  denotes the  $i$ th data point in the neighbourhood that satisfies the condition  $c$ ,  $i \in [1, N]$ , and  $f_\theta$  is the pre-trained registration network Voxelmorph with weights  $\theta$  that estimates the transformation between the population atlas and every neighbouring image. The final

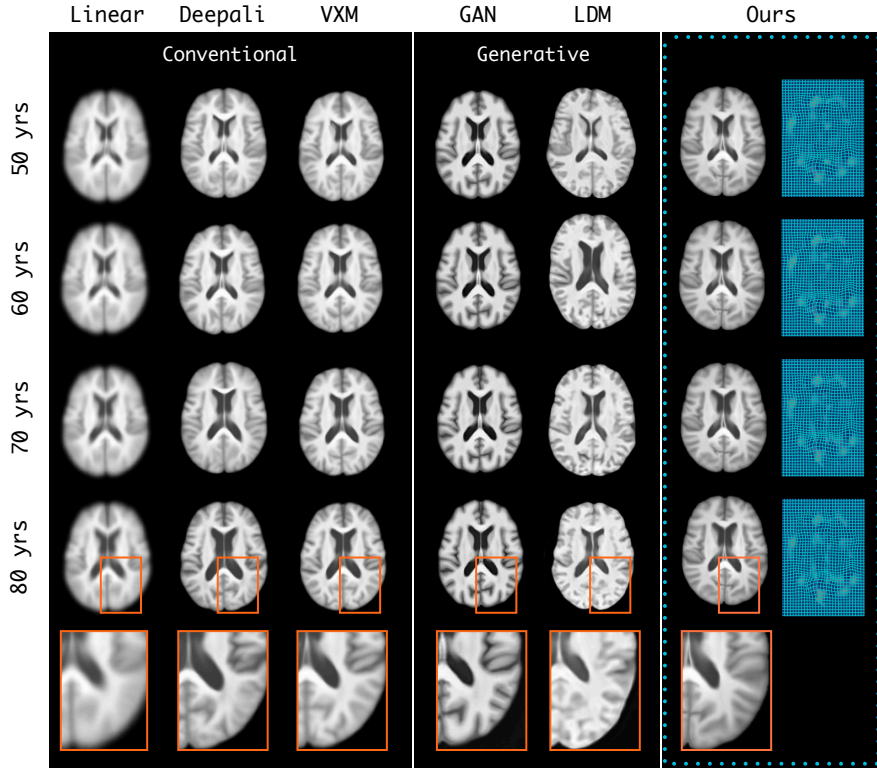


Fig. 2: Qualitative results of the proposed method (right) and baselines conditioned on ages 50 to 80 years old. Our method is the only one generating displacement fields (most right column). Regions of interest are displayed in the bottom row, demonstrating more details of the atlases.

objective is a linear combination of the diffusion loss  $\mathcal{L}_{\text{diff}}$ , the geometry preserving loss  $\mathcal{L}_{\text{geom}}$  and the bending energy, a second order derivative regularisation term  $\mathcal{R}$  [28], which enforces smoothness on the deformation field. Finally,  $\lambda_1, \lambda_2$  are weighting factors controlling each component's contribution to the overall objective:

$$\mathcal{L} = \mathcal{L}_{\text{diff}} + \lambda_1 \mathcal{L}_{\text{geom}} + \lambda_2 \mathcal{R}. \quad (2)$$

## 4 Experimental Setup

**Dataset** We use 5000 (4000 training / 300 validation / 700 testing) T1-weighted Magnetic Resonance Images (MRI) of brains from the UK Biobank [32] dataset. The brain images have an isotropic spacing of  $1\text{mm}^3$  and a size of  $(160 \times 225 \times$

160). All images are skull-stripped using BET [29], rigidly registered to a common MNI space [13] using the conventional registration framework Deepali [1] and segmented using FAST [36]. As conditions, we use the subjects' age, ranging from 50 to 80 years old and the cerebrospinal fluid (CSF) volume normalised by the total number of voxels, ranging from 0.0 to 0.6. As a general population atlas, we use the publicly available MNI ICBM152 template [13]. We furthermore use 5000 whole-body MRI from the UK Biobank [32]. We process the stitched [19] water contrast images with a resolution of  $(2.23 \times 3 \times 2.23) \text{ mm}^3$  and size  $(224 \times 168 \times 363)$  and downsample them by a factor of 2. As conditions, we categorise BMI groups following [31]. As a general population atlas, we use two of the available atlases for healthy males and females proposed by [31].

**Implementation** We implement the AE and the LDM following [27,24] using the publicly available repository [23]. To keep the memory requirements tractable, we randomly sample a neighbourhood of 25 images that satisfy the condition at every epoch. During the hyperparameter tuning process, the optimal results were attained by assigning equal weights to both the diffusion and structure-preserving loss components and 0.5 for the regularisation term. Implementation details regarding the AE, LDM, Voxelmorph, and the baseline hyperparameters can be found in the appendix Table 3. We train all networks on an A100 80GB GPU with Pytorch. The source code is publicly available<sup>5</sup>.

**Baselines** We compare our method to five related approaches for atlas generation. We evaluate three widely used *unconditional* atlas construction algorithms: (1) a linear average of the images, (2) Deepali [1], an iterative optimisation registration framework, and (3) Voxelmorph [6], a learning-based method. Since these methods are unconditional, we sample, register, and average 1000 subjects for every condition to produce atlases. Furthermore, we use two *conditional* learning-based methods. We investigate (4) a GAN-based method [12] that consists of a conditional generator to produce the desired atlases that are registered to every image in the dataset and a discriminator to ensure a realistic appearance. Finally, we extend (5) a vanilla LDM [24] with our morphology-preserving module to enable it to generate atlases. This is a direct ablation of our proposed method, which generates deformation fields.

## 5 Results and Discussion

The optimal conditional atlas should minimise the distance to every subject that satisfies the condition without deviating from the dataset appearance in the intensity domain. We measure this with metrics quantifying similarities in appearance, structural properties, and centrality.

Figure 2 illustrates the resulting brain atlases of the different methods conditioned on age. Comparing our method to the conventionally generated atlases,

---

<sup>5</sup> <https://anonymous.4open.science/r/diffdef/README.md>

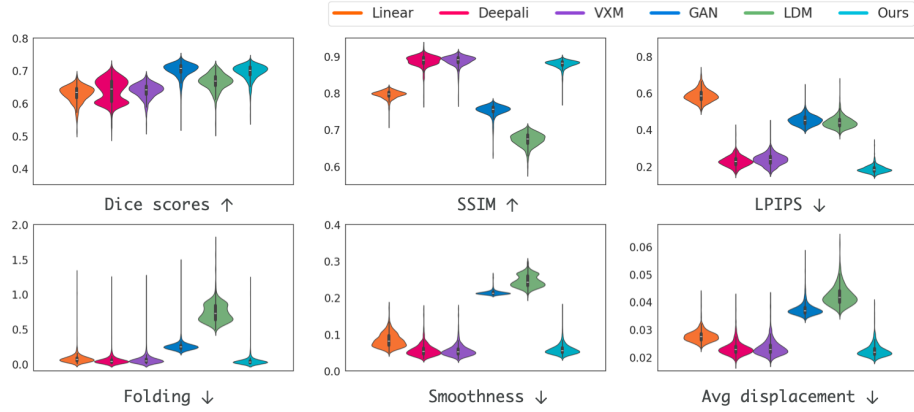


Fig. 3: **Age** conditioned atlases evaluation metrics against a test set. The SSIM (top middle) and LPIPS (top right) scores show perceptual similarity to the test set. Folding, smoothness, average displacement (bottom row) and dice scores (top left) exhibit structural proximity.

we achieve sharper boundaries while maintaining the intensity distribution of the dataset and the overall brain shape. Since our method deforms an existing population atlas with the generated deformation field, it does not introduce any hallucinations or unrealistic intensities, e.g. darker ventricles. On the other hand, GAN and LDM are prone to generate unrealistic intensities and noisy backgrounds, requiring further post-processing and brain shapes. Atrophy of the lateral ventricles is a well-studied biomarker in neurological aging [17]. This is visible in all three conventional methods and our approach, while GAN and LDM fail to capture this effect consistently. Furthermore, our approach is the only one that generates a deformation field (most right column Figure 2). This inherently enhances the interpretability of our method, allowing us to localise structural changes. More qualitative results can be found in Figure 5 in the appendix.

Several quantitative measures corroborate these findings, summarised in Figure 3 and Tables 1, 2 in the appendix. For this, we select a test set of 100 images per condition, which we register to each conditional atlas, resulting in a deformation field  $\mathcal{T}_i$  for each image. We analyse the centrality of the atlas by comparing the average norms of the displacements ( $\frac{1}{100} \sum_i \|\mathcal{T}_i\|$ ), the spatial smoothness with the magnitude of the gradient of the transformations' Jacobian determinant ( $|\nabla J|$ ) and the foldings with the ratio of points with  $J < 0$ . Our framework performs on par with the conventional methods while outperforming the other generative models, GAN and LDM (second row of Figure 3). Additionally, we segment the population atlas [13] using FAST segmentation algorithm [36] to obtain the CSF, white, and grey matter labels, which we propagate to the generated atlases via deformable registration. We assess structural plausibility by measuring the Dice overlap of the conditional atlases with each image of the test set. To evaluate the appearance of the atlases, we employ the Structural Sim-

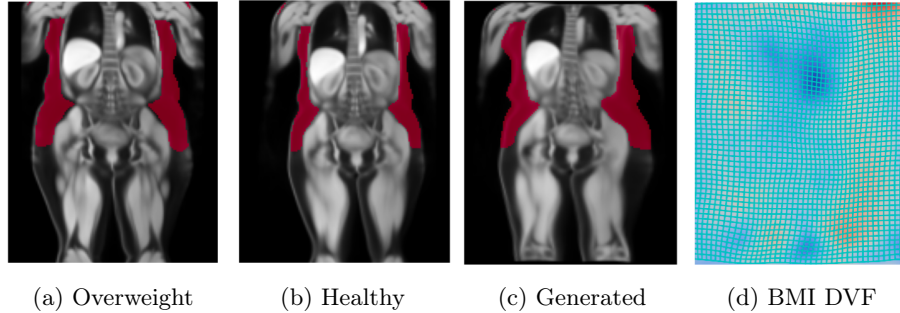


Fig. 4: The healthy female atlas (b) is deformed by the conditional DVF (d) to generate the overweight female atlas (c). The deformation field (d) showcases the expansion regions, where we observe a subcutaneous fat increase (red label). (a) shows the ground truth of the overweight female atlas.

ilarity Index Measure (SSIM) [34] and the Perceptual Image Patch Similarity (LPIPS) [35]. Our method demonstrates superiority in the perceptual metrics compared to GAN and LDM without a post-processing denoising step.

The applicability of our method is not limited to brain datasets. In Figure 4, we showcase qualitative results of generated whole-body atlases. In this case, the female overweight atlas (4c) is generated by applying the deformation field conditioned on BMI (4d) to a healthy BMI atlas (4b). We demonstrate how the deformation field can be used to localise the increase in subcutaneous fat (red segmentation mask), resulting in a generated overweight atlas, which is very similar to the conventionally created one (4a).

## 6 Conclusion

Atlases generated with conventional methods are well-established due to their reliability and realism. They, however, face scalability issues in terms of speed, data, and memory requirements, which renders them difficult to use with sub-population conditioning. Others have used generative modelling to synthesise conditional atlases, which is faster and not as dependent on the feature selection but this comes with other limitations such as training instabilities and mode collapse [21]. In this work, we propose to combine the highly interpretable deformation vector field from the conventional methods and the power of diffusion models to generate deformation fields to transform an existing population atlas into conditioned ones. Our proposed method outperforms previous approaches in terms of structural and perceptual aspects. However, our method is dependent on the input population atlas. In the case of the brain, this poses a minimal issue as there are plenty of general atlases available. Nevertheless, in the case of whole-body, atlas definition and construction are more challenging due to the high anatomical variability. Another challenge is that our method requires long

training. Conversely, it can generate conditional atlases in seconds. Finally, it is not tailored to a specific image modality; one could learn to generate an atlas on a T1-weighted dataset and seamlessly extend it to another modality, e.g. T2-weighted.

## 7 Acknowledgements

This research has been conducted using the UK Biobank dataset under the application number 87802. T.M. and S.S. were supported by the ERC (Deep4MI - 884622). SS has furthermore been supported by BMBF and the NextGenerationEU of the European Union. The authors gratefully acknowledge the scientific support and HPC resources provided by the Erlangen National High Performance Computing Center (NHR@FAU) of the Friedrich-Alexander-Universität Erlangen-Nürnberg (FAU). The hardware is funded by the German Research Foundation (DFG)

## References

1. deepali: Image, point set, and surface registration in pytorch. <https://doi.org/10.5281/zenodo.8170161>, <https://biomedia.github.io/deepali/>
2. Alloussonnière, S., Amit, Y., Trouvé, A.: Towards a coherent statistical framework for dense deformable template estimation. *Journal of the Royal Statistical Society Series B: Statistical Methodology* **69**(1), 3–29 (2007)
3. Arjovsky, M., Chintala, S., Bottou, L.: Wasserstein generative adversarial networks. In: ICML. pp. 214–223. PMLR (2017)
4. Avants, B., Gee, J.: Geodesic estimation for large deformation anatomical shape averaging and interpolation. *NeuroImage* **23**, S139–S150 (2004)
5. Avants, B., Yushkevich, P., Pluta, J., Minkoff, D., Korczykowski, M., Detre, J., Gee, J.: The optimal template effect in hippocampus studies of diseased populations. *NeuroImage* **49**(3), 2457–2466 (2010)
6. Balakrishnan, G., Zhao, A., Sabuncu, M.R., Guttag, J., Dalca, A.V.: Voxelmorph: a learning framework for deformable medical image registration. *TMI* **38**(8), 1788–1800 (2019)
7. Bercea, C.I., Neumayr, M., Rueckert, D., Schnabel, J.A.: Mask, stitch, and resample: Enhancing robustness and generalizability in anomaly detection through automatic diffusion models. In: ICML Workshop (2023), <https://openreview.net/forum?id=kTpafpXrq>
8. Bhatia, K.K., Hajnal, J.V., Puri, B.K., Edwards, A.D., Rueckert, D.: Consistent groupwise non-rigid registration for atlas construction. In: 2004 2nd IEEE International Symposium on Biomedical Imaging: Nano to Macro (IEEE Cat No. 04EX821). pp. 908–911. IEEE (2004)
9. Croitoru, F., Hondru, V., Ionescu, R.T., Shah, M.: Diffusion models in vision: A survey. *TPAMI* (2023)
10. Dalca, A., Rakic, M., Guttag, J., Sabuncu, M.: Learning conditional deformable templates with convolutional networks. *NeurIPS* **32** (2019)
11. Davis, B., Lorenzen, P., Joshi, S.C.: Large deformation minimum mean squared error template estimation for computational anatomy. In: ISBI. vol. 4, pp. 173–176 (2004)

12. Dey, N., Ren, M., Dalca, A., Gerig, G.: Generative adversarial registration for improved conditional deformable templates. In: ICCV. pp. 3929–3941 (2021)
13. Grabner, G., Janke, A.L., Budge, M.M., Smith, D., Pruessner, J., Collins, D.L.: Symmetric atlasing and model based segmentation: an application to the hippocampus in older adults. In: MICCAI. pp. 58–66. Springer (2006)
14. Gulrajani, I., Ahmed, F., Arjovsky, M., Dumoulin, V., Courville, A.: Improved training of wasserstein gans. NeurIPS **30** (2017)
15. Ho, J., Jain, A., Abbeel, P.: Denoising diffusion probabilistic models. NeurIPs **33**, 6840–6851 (2020)
16. Joshi, S., Davis, B., Jomier, M., Gerig, G.: Unbiased diffeomorphic atlas construction for computational anatomy. NeuroImage **23**, S151–S160 (2004)
17. Kaye, J., DeCarli, C., Luxenberg, J., Rapoport, S.: The significance of age-related enlargement of the cerebral ventricles in healthy men and women measured by quantitative computed x-ray tomography. Journal of the American Geriatrics Society **40**(3), 225–231 (1992)
18. Kim, B., Han, I., Ye, J.: Diffusemorph: unsupervised deformable image registration using diffusion model. In: ECCV. pp. 347–364. Springer (2022)
19. Lavdas, I., Glocker, B., Rueckert, D., Taylor, S., Aboagyi, E.E., Rockall, A.: Machine learning in whole-body mri: experiences and challenges from an applied study using multicentre data. Clinical Radiology (2019)
20. Li, L., Sinclair, M., Makropoulos, A., Hajnal, J., David E., A., Kainz, B., Rueckert, D., Alansary, A.: Cas-net: conditional atlas generation and brain segmentation for fetal mri. In: UNSURE MICCAI Workshop. pp. 221–230. Springer (2021)
21. Mescheder, L.: On the convergence properties of gan training. arXiv preprint arXiv:1801.04406 **1**, 16 (2018)
22. Paulsen, J., Langbehn, D., Stout, J., Aylward, E., Ross, C., Nance, M., Guttman, M., Johnson, S., MacDonald, M., Beglinger, L., et al.: Detection of huntington’s disease decades before diagnosis: the predict-hd study. Journal of Neurology, Neurosurgery & Psychiatry **79**(8), 874–880 (2008)
23. Pinaya, W.H., Graham, M.S., Kerfoot, E., Tudosiu, P., Dafflon, J., Fernandez, V., Sanchez, P., Wolleb, J., da Costa, P., Patel, A., et al.: Generative ai for medical imaging: extending the monai framework. arXiv preprint arXiv:2307.15208 (2023)
24. Pinaya, W., Tudosiu, P., Dafflon, J., Da Costa, P., Fernandez, V., Nachev, P., Ourselin, S., Cardoso, M.: Brain imaging generation with latent diffusion models. In: MICCAI Workshop on Deep Generative Models. pp. 117–126. Springer (2022)
25. Qin, Y., Li, X.: Fsdifffreg: Feature-wise and score-wise diffusion-guided unsupervised deformable image registration for cardiac images. In: MICCAI. pp. 655–665. Springer (2023)
26. Qiu, H., Qin, C., Schuh, A., Hammerink, K., Rueckert, D.: Learning diffeomorphic and modality-invariant registration using b-splines. In: MIDL (2021)
27. Rombach, R., Blattmann, A., Lorenz, D., Esser, P., Ommer, B.: High-resolution image synthesis with latent diffusion models. In: CVPR. pp. 10684–10695 (2022)
28. Rueckert, D., Sonoda, L., Hayes, C., Hill, D., Leach, M., Hawkes, D.: Nonrigid registration using free-form deformations: application to breast mr images. TMI **18**(8), 712–721 (1999)
29. Smith, S.: Bet: Brain extraction tool. FMRIB TR00SMS2b, Oxford Centre for fMRI of the Brain), Department of Clinical Neurology, Oxford University, John Radcliffe Hospital, Headington, UK p. 25 (2000)
30. Sotiras, A., Davatzikos, C., Paragios, N.: Deformable medical image registration: A survey. TMI **32**, 1153–1190 (2013)

31. Starck, S., Sideri-Lampretsa, V., Ritter, J., Zimmer, V., Braren, R., Mueller, T., Rueckert, D.: Constructing population-specific atlases from whole body mri: Application to the ukbb. PREPRINT (Version 1) available at Research Square (2023). <https://doi.org/10.21203/rs.3.rs-3303755/v1>
32. Sudlow, C., Gallacher, J., Allen, N., Beral, V., Burton, P., Danesh, J., Downey, P., Elliott, P., Green, J., Landray, M., et al.: Uk biobank: an open access resource for identifying the causes of a wide range of complex diseases of middle and old age. *PLoS medicine* **12**(3), e1001779 (2015)
33. Thompson, P., Woods, R., Mega, M., Toga, A.: Mathematical/computational challenges in creating deformable and probabilistic atlases of the human brain. *Human Brain Mapping* **9**(2), 81–92 (2000)
34. Wang, Z., Bovik, A., Sheikh, H., Simoncelli, E.: Image quality assessment: from error visibility to structural similarity. *TMI* **13**(4), 600–612 (2004)
35. Zhang, R., Isola, P., Efros, A., Shechtman, E., Wang, O.: The unreasonable effectiveness of deep features as a perceptual metric. In: *CVPR*. pp. 586–595 (2018)
36. Zhang, Y., Brady, M., Smith, S.: Segmentation of brain mr images through a hidden markov random field model and the expectation-maximization algorithm. *TMI* **20**(1), 45–57 (2001)

## 8 Appendix

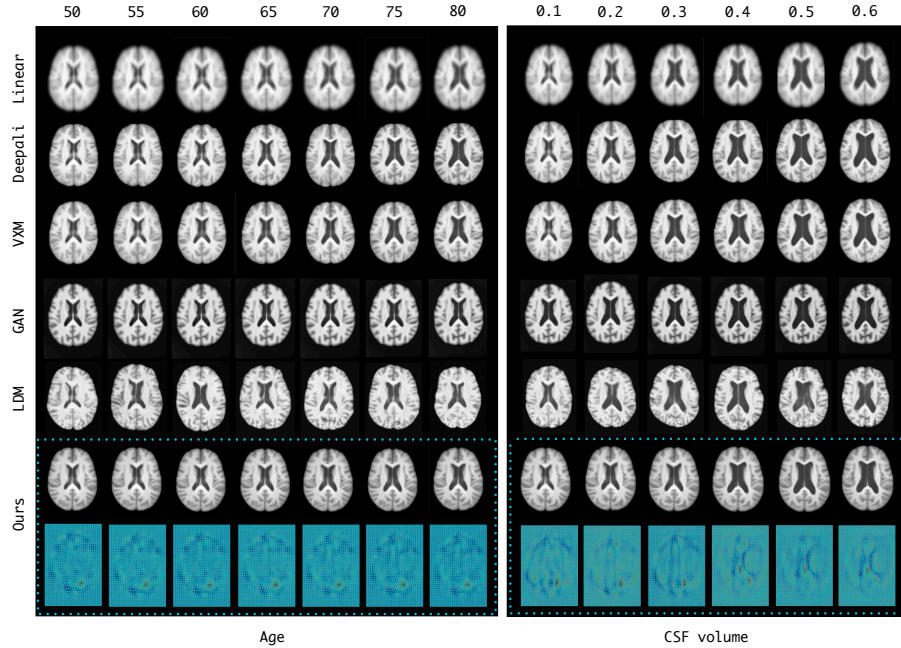


Fig. 5: Overview of all atlases across age and normalised cerebrospinal fluid (CSF) volume conditioning. Each row shows one method and each column the associated condition.

Table 1: Overall pairwise results between the generated atlases and a test set of 100 images for each condition. The best results are highlighted in **bold** and the second best are underlined.

	DSC $\uparrow$	Folding (%) $\downarrow$	$ \nabla_J  \downarrow$	Avg. disp. $\ \Phi\  \downarrow$	LPIPS $\downarrow$	SSIM $\uparrow$
Age	Lin 0.57 $\pm$ 0.005	0.08 $\pm$ 0.09	0.028 $\pm$ 0.0022	8414 $\pm$ 1924	0.59 $\pm$ 0.034	0.80 $\pm$ 0.012
	<b>DLI</b> 0.58 $\pm$ 0.123	<u>0.05 <math>\pm</math> 0.08</u>	<u>0.023 <math>\pm</math> 0.0026</u>	5645 $\pm$ 1664	0.23 $\pm$ 0.030	<b>0.89 <math>\pm</math> 0.016</b>
	VXM 0.57 $\pm$ 0.008	0.06 $\pm$ 0.09	<u>0.023 <math>\pm</math> 0.0029</u>	<b>5555 <math>\pm</math> 1644</b>	0.24 $\pm$ 0.032	<b>0.89 <math>\pm</math> 0.015</b>
	GAN <b>0.66 <math>\pm</math> 0.009</b>	0.26 $\pm$ 0.09	0.037 $\pm$ 0.0025	21399 $\pm$ 726	0.45 $\pm$ 0.027	0.75 $\pm$ 0.016
	LDM 0.58 $\pm$ 0.015	0.74 $\pm$ 0.14	0.042 $\pm$ 0.0037	24588 $\pm$ 1683	0.44 $\pm$ 0.031	0.67 $\pm$ 0.018
	Ours <b>0.65 <math>\pm</math> 0.007</b>	<b>0.04 <math>\pm</math> 0.08</b>	<b>0.022 <math>\pm</math> 0.0025</b>	5877 $\pm$ 1552	<b>0.19 <math>\pm</math> 0.021</b>	<u>0.88 <math>\pm</math> 0.013</u>
CSF	Lin 0.50 $\pm$ 0.098	0.09 $\pm$ 0.12	0.029 $\pm$ 0.0029	8186 $\pm$ 2111	0.560 $\pm$ 0.043	0.79 $\pm$ 0.015
	<b>DLI</b> 0.61 $\pm$ 0.091	<u>0.07 <math>\pm</math> 0.12</u>	<u>0.025 <math>\pm</math> 0.0035</u>	5842 $\pm$ 1871	0.25 $\pm$ 0.030	<b>0.88 <math>\pm</math> 0.020</b>
	VXM 0.63 $\pm$ 0.097	0.08 $\pm$ 0.12	<u>0.025 <math>\pm</math> 0.0037</u>	<b>5682 <math>\pm</math> 1834</b>	<u>0.24 <math>\pm</math> 0.032</u>	<b>0.88 <math>\pm</math> 0.019</b>
	GAN 0.64 $\pm$ 0.118	0.36 $\pm$ 0.17	0.039 $\pm$ 0.0036	21998 $\pm$ 1064	0.44 $\pm$ 0.033	0.72 $\pm$ 0.010
	LDM 0.58 $\pm$ 0.138	0.80 $\pm$ 0.15	0.043 $\pm$ 0.0034	24676 $\pm$ 2141	0.45 $\pm$ 0.036	0.67 $\pm$ 0.021
	Ours <b>0.66 <math>\pm</math> 0.089</b>	<b>0.06 <math>\pm</math> 0.12</b>	<b>0.024 <math>\pm</math> 0.0032</b>	6134 $\pm$ 1691	<b>0.20 <math>\pm</math> 0.027</b>	<u>0.87 <math>\pm</math> 0.018</u>

Table 2: Evaluation criteria and their description. All these metrics are performed between an atlas and the registered dataset.

Metric	Category	Evaluated on	Description
Dice Score	Structure	Segmentation labels	Measuring the overlap of labels between the generated atlas and the registered images
Folding ratio	Structure	DVF	Number of voxels with negative Jacobian determinant
Smoothness	Structure	DVF	The magnitude of the gradient of the transformation’s Jacobian determinant
Average disp.	Structure	DVF	The average norms of the DVFs
SSIM	Appearance	Registered Images	Index computed between the generated atlas and the registered images
LPIPS	Appearance	Registered Images	Metric computed on patches between the generated atlas and the registered images

Table 3: Selected hyperparameters for each method. We refer the reader to the relevant papers for further details regarding the architectural choices.

	Deepali	GAN	VXM	AE	LDM
Learning Rate	$10^{-3}$	$10^{-4}$	$10^{-4}$	$5e^{-5}$	$2.5^{-5}$
Batch Size	-	1	8	1	1
Loss	MSE	Adversarial & MSE	Cross-Correlation	L1 & Perceptual & KL Div.	MSE
Diffeomorphisms	Yes	No	No	-	-
Res. levels	3	1	1	1	1
Regularisation	0.1	$10^{-3}$	0.1	-	-
Further details	[1]	[12]	[26]	[23]	[23]